Electronic Supplementary Information

Cation exchange MOF-derived nitrogen-doped porous carbons for CO_2 capture and supercapacitor electrode materials

Ying Pan,[a] Yuxin Zhao,[b] Shanjun Mu,[b] Yu Wang,[a] Chunming Jiang,[b] Quanzhen Liu,[b] Qianrong Fang,[a] Ming Xue,*[a] and Shilun Qiu[a]

[a]*State Key Laboratory of Inorganic Synthesis and Preparative Chemistry, Jilin University, Changchun 130012, P. R. China.*

[b]*State Key Laboratory of Safety and Control for Chemicals, SINOPEC Research Institute of Safety Engineering, Shandong Qingdao, 266101, P. R. China.*

**Corresponding author: M. Xue, Email: xueming@jlu.edu.cn*

Table of Contents

1. Powder X-ray Diffraction and Thermogravimetric Analysis

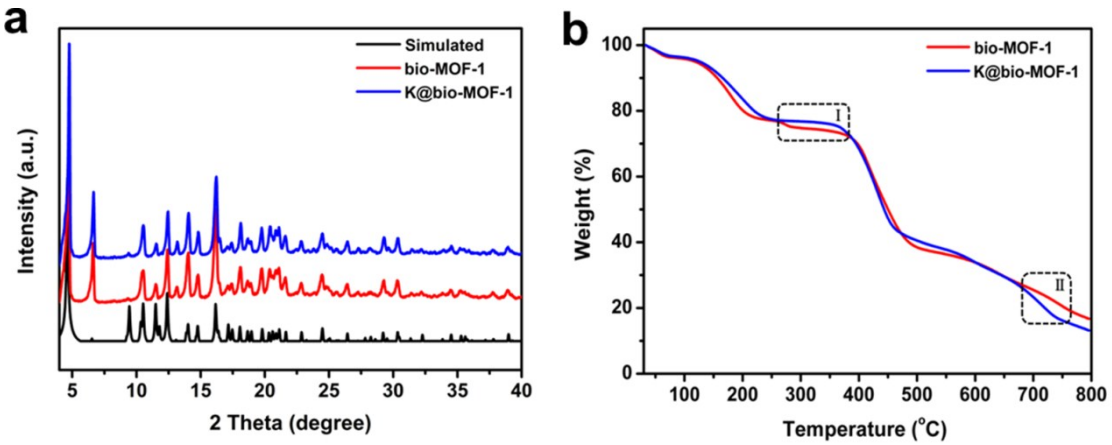

Figure S1. (a) PXRD patterns of the simulated single crystal crystallography data (black), the as-synthesized bio-MOF-1 (red) and K@bio-MOF-1 (blue), and (b) TGA curves of bio-MOF-1 (red) and K@bio-MOF-1 (blue).

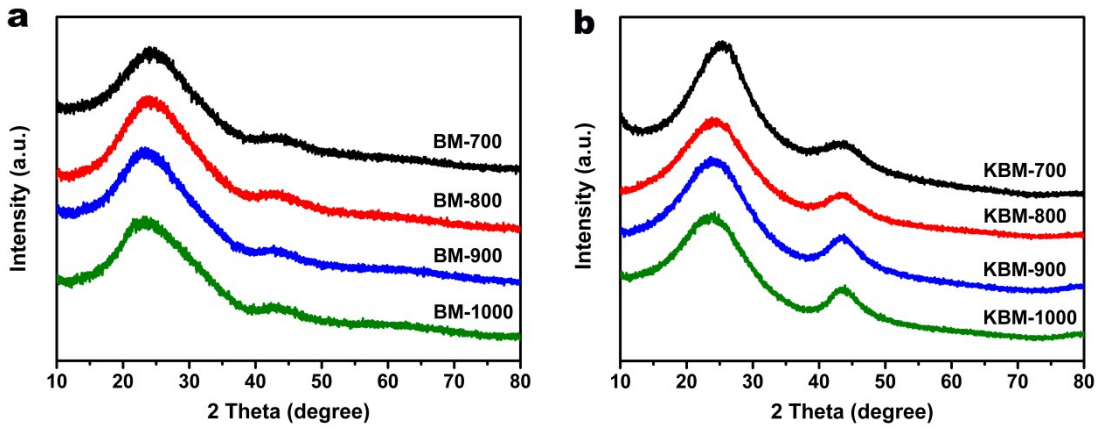

Figure S2. Powder XRD patterns of (a) bio-MOF-1 derived porous carbons and (b) K@bio-MOF-1 derived porous carbons.

2. Morphological characterization and EDS analysis

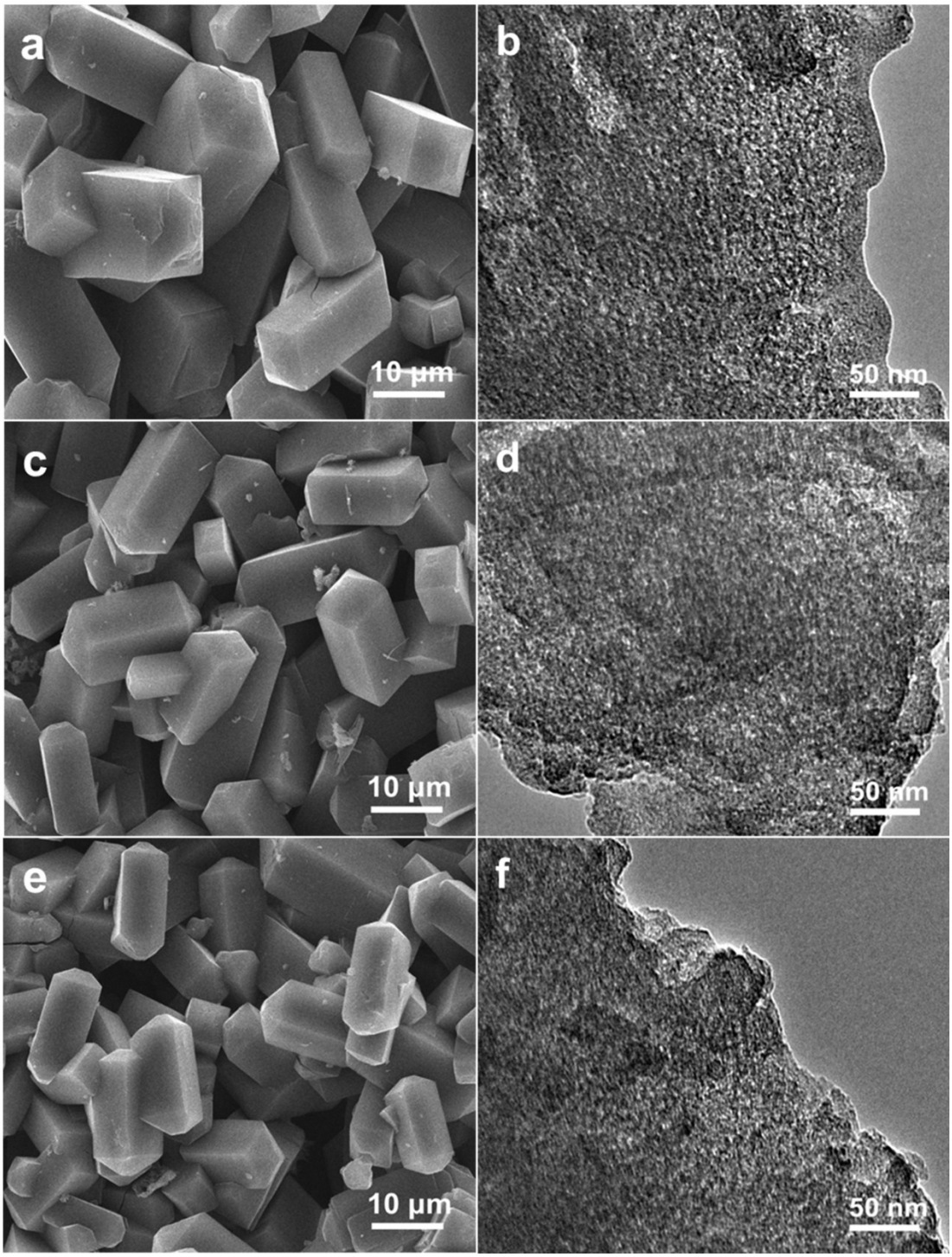

Figure S3. SEM and TEM images of (a, b) BM-800, (c, d) BM-900, (e, f) BM-1000.

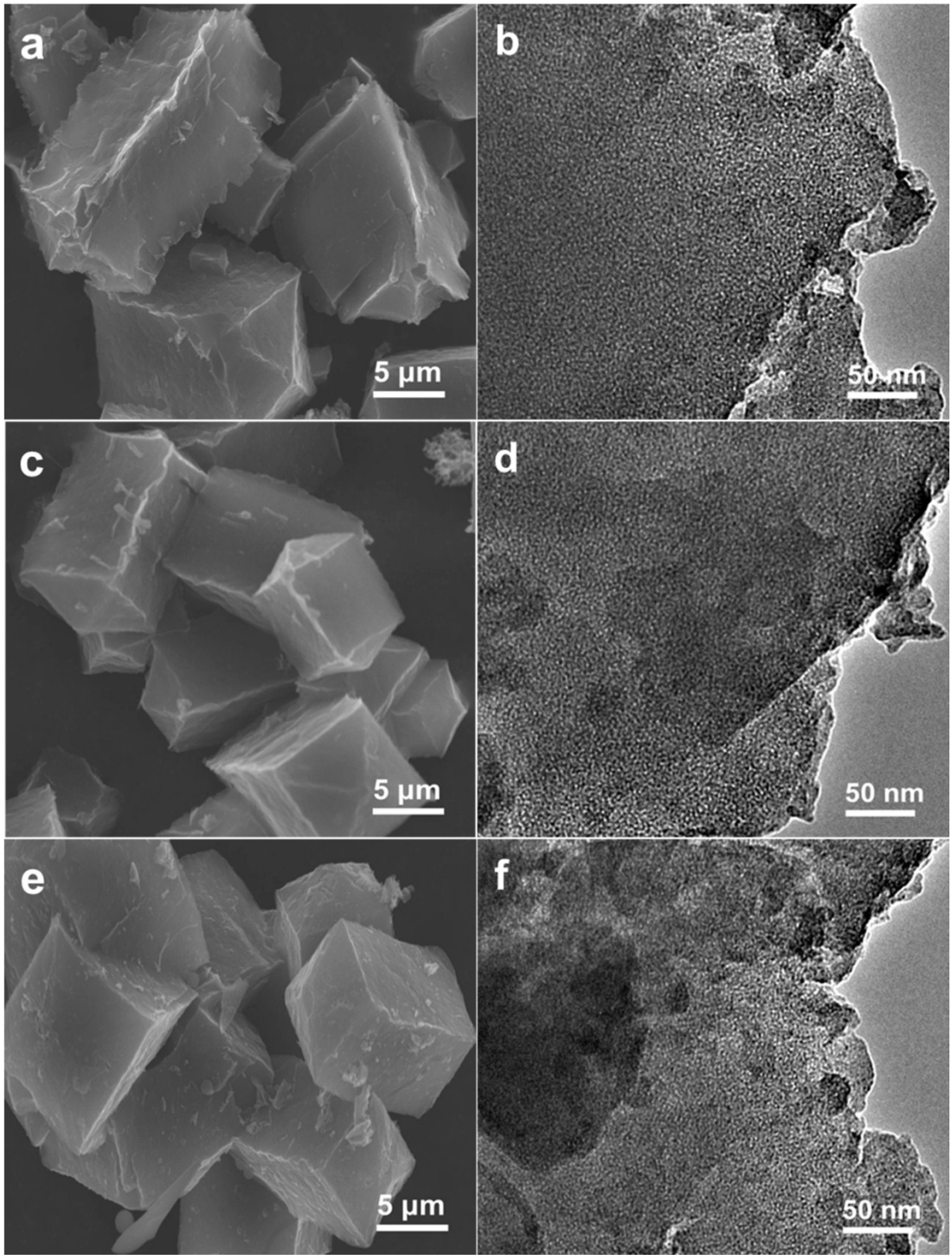

Figure S4. SEM and TEM images of (a, b) KBM-800, (c, d) KBM-900, (e, f) KBM-1000.

3. Energy dispersive spectrometer (EDS) Analysis

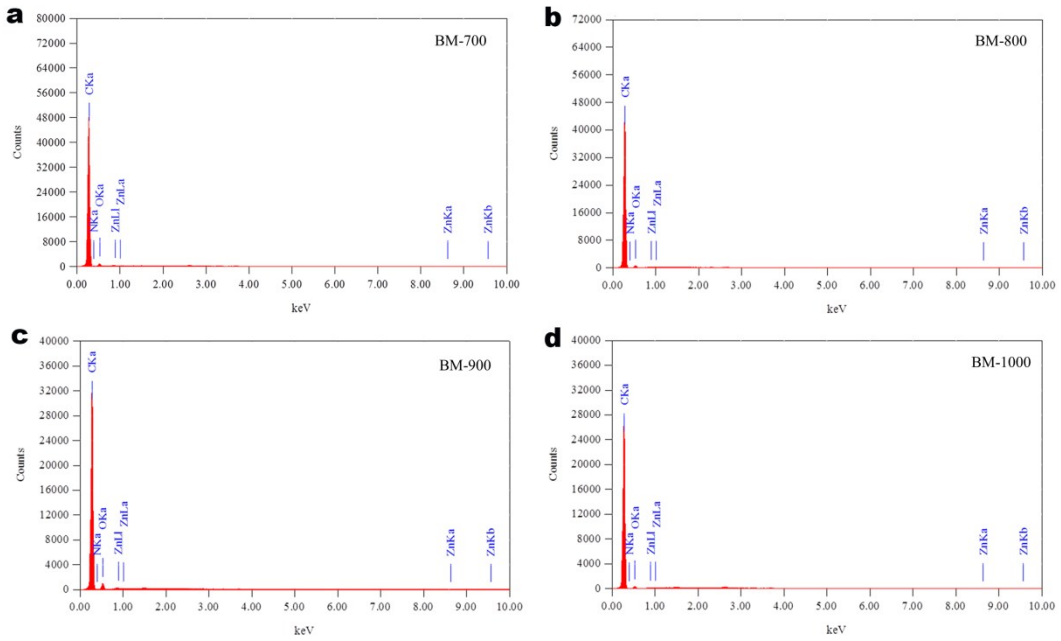

Figure S5. EDS spectra of (a) BM-700, (b) BM-800, (c) BM-900 and (d) BM-1000.

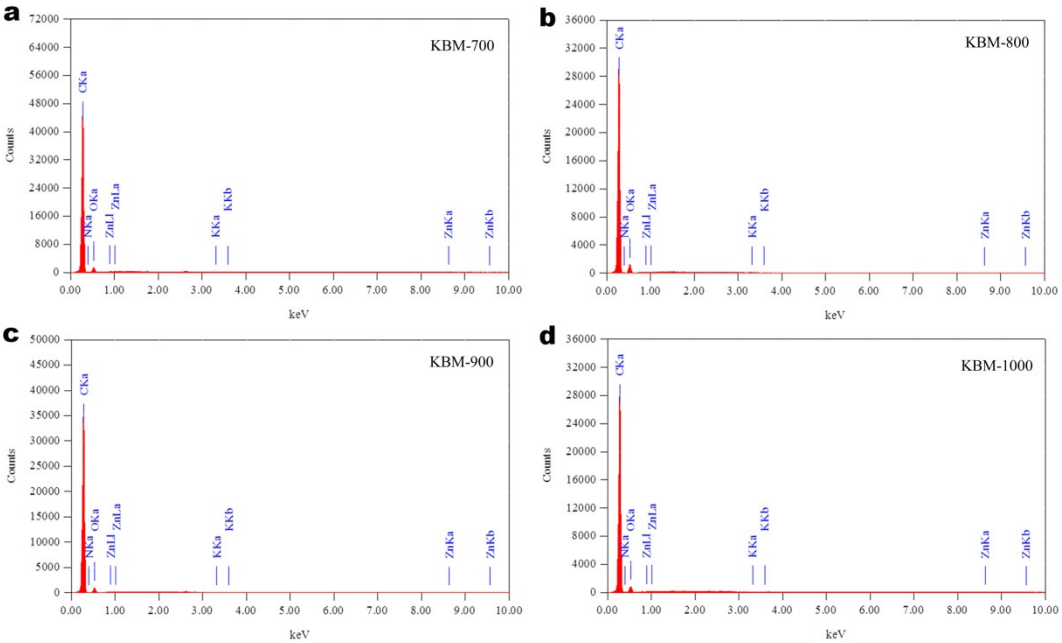

Figure S6. EDS spectra of (a) KBM-700, (b) KBM-800, (c) KBM-900 and (d) KBM-1000.

4. Gas Adsorption Measurements

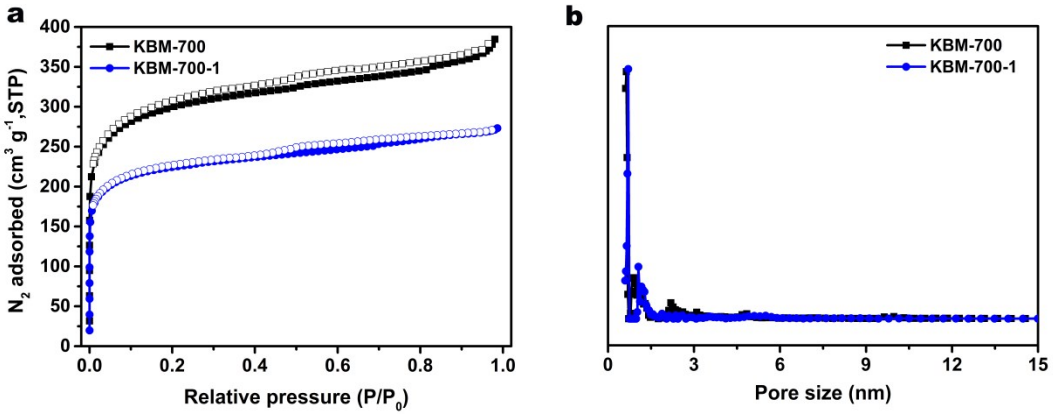

Figure S7. Nitrogen adsorption-desorption isotherms of (a) KBM-700 and KBM-700-1 at 77 K, and (b) the corresponding pore size distribution curves of the KBM-700 and KBM-700-1 samples.

Table S1. Textural properties of KBM-700 and KBM-700-1.

Sample	S_{BET} $m^2\ g^{-1}$	V_{total} $cm^3\ g^{-1}$	V_{micro} $cm^3\ g^{-1}$	Pore size (nm)
KBM-700	1129	0.55	0.40	0.64
KBM-700-1	855	0.39	0.30	0.70

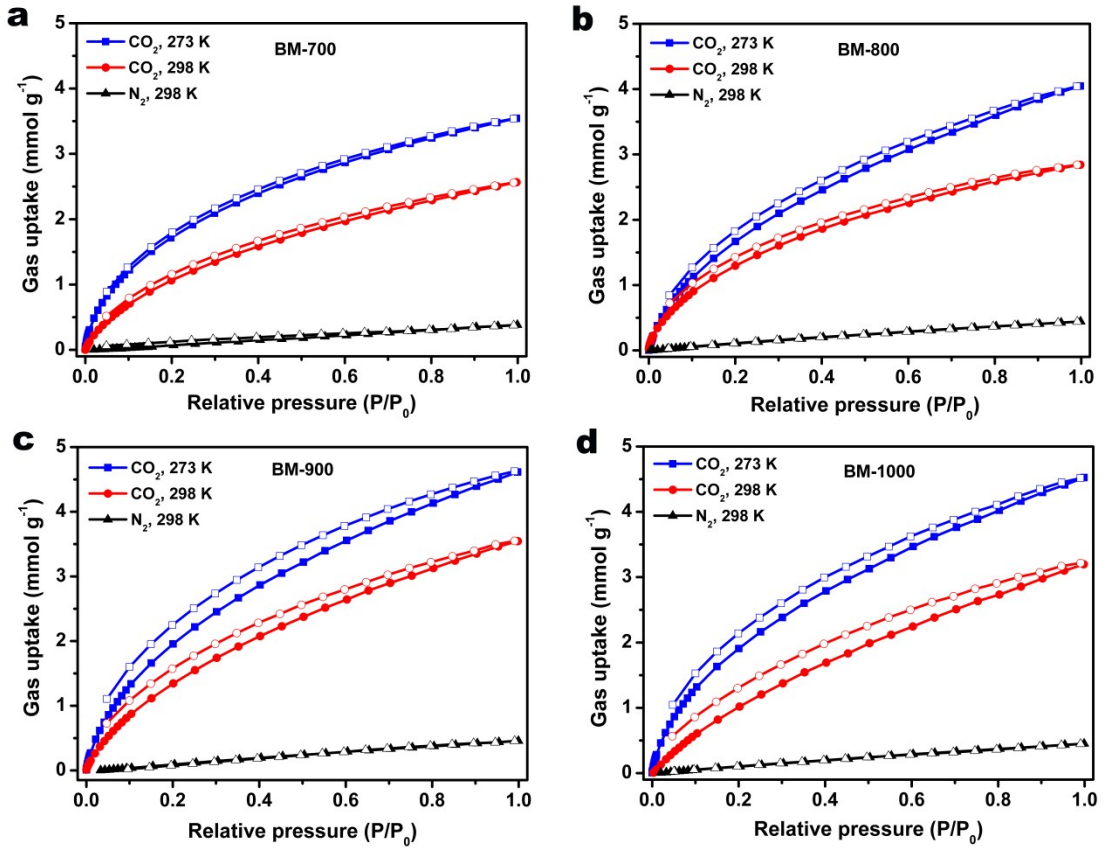

Figure S8. Gas sorption capacities for (a) BM-700, (b) BM-800, (c) BM-900 and (d) BM-1000, CO_2 at 273 K (blue square), 298 K (red circular) and N_2 at 298 K (black triangle).

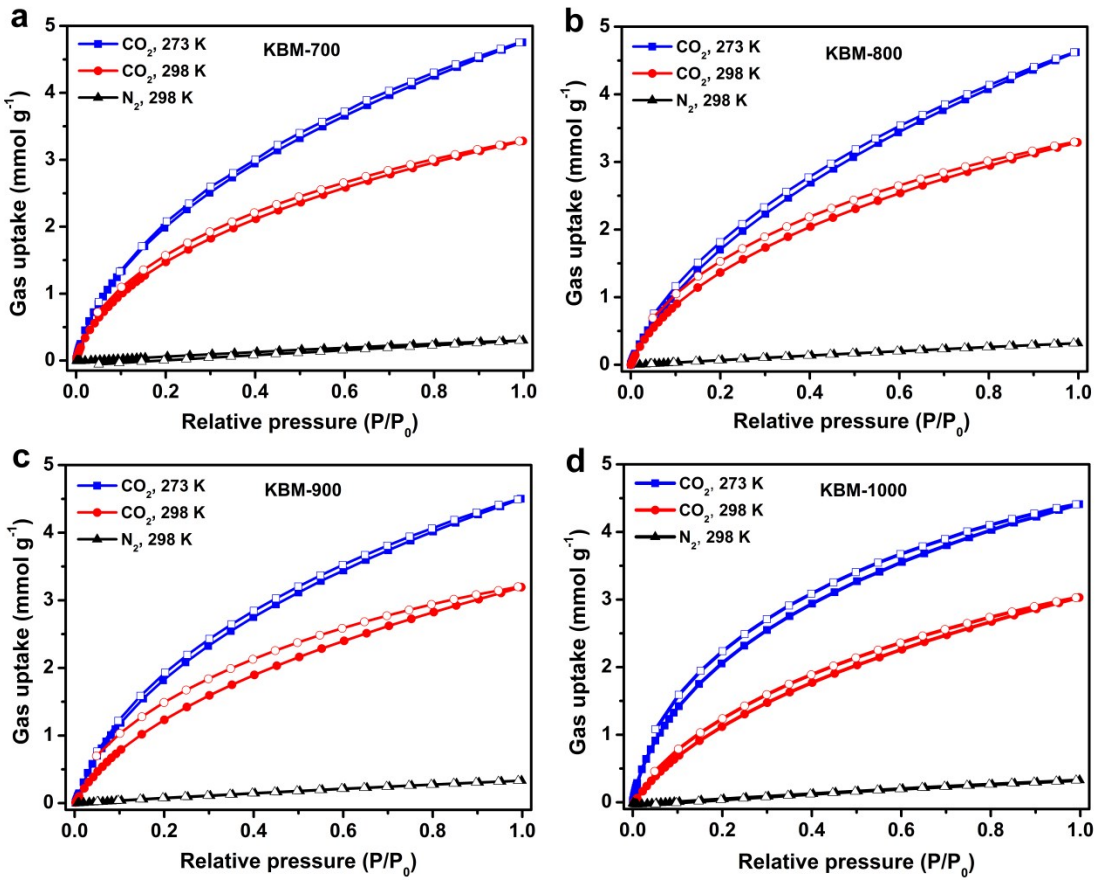

Figure S9. Gas sorption capacities for (a) KBM-700, (b) KBM-800, (c) KBM-900 and (d) KBM-1000, CO_2 at 273 K (blue square), 298 K (red circular) and N_2 at 298 K (black triangle).

5. Calculation of heats of adsorption

Isosteric heat of adsorption (Q_{st}) for all the **BM-*T*** and **KBM-*T*** samples were calculated using the CO_2 sorption isotherms measured at 273 and 298 K based on the Clausius-Clapeyron equation using the ASiQwin software installed in Quantachrome Autosorb-iQ2 instruments. Clausius-Clapeyron equation is in the form:

$$ln\left(\frac{p_2}{p_1}\right) = \frac{Q_{st}}{R}\left(\frac{1}{T_1} - \frac{1}{T_2}\right)$$

where Q_{st} is the isosteric heats of adsorption, T_i represents a temperature at which an isotherm i is measured, p_i represents a pressure at which a specific equilibrium adsorption amount is reached at T_i, R is the universal gas constant (8.314 J K^{-1} mol^{-1}).

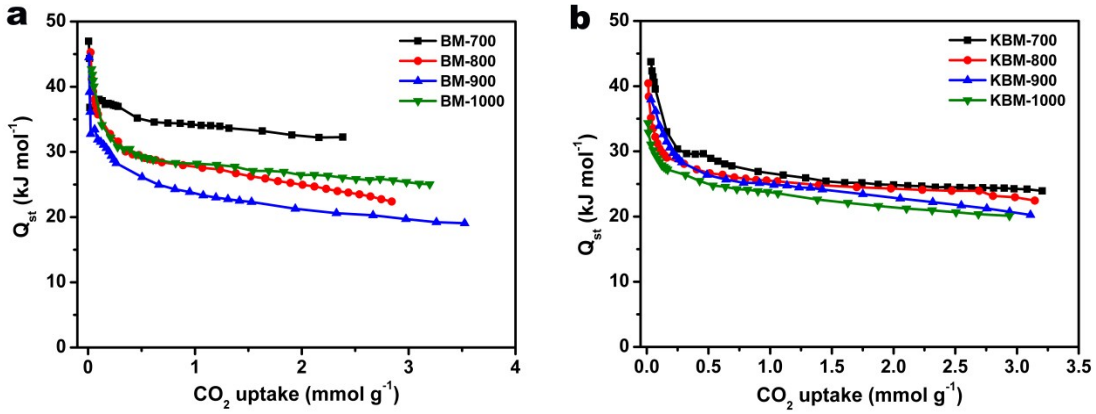

Figure S10. Isosteric heat of adsorption (Q_{st}) of (a) bio-MOF-1 derived porous carbons, (b) K@bio-MOF-1 derived porous carbons calculated using the Clausius−Clapeyron equation, based on the CO_2 adsorption isotherms at 273, 298 K.

6. IAST Selectivity Analysis

Ideal Adsorption Solution Theory (IAST)

We used the IAST of Myers and Prausnitz[1,2] along with the single-component adsorption isotherm fits to determine the molar loadings in the mixture for specified partial pressures in bulk phases. The excess adsorption data for pure CO_2, N_2 measured at 298 K, were first converted to absolute loadings using the Peng-Robinson equation of state for estimation of the fluid densities. The absolute component loadings at 298 K were fitted using the single-site Langmuir-Freundlich model. The fitted constants are listed in Table S1.

The single-site Langmuir-Freundlich model can be expressed as follows:

$$N = A_1 \times \frac{b_1 p^{c_1}}{1 + b_1 p^{c_1}} \quad (1)$$

where A_1 is saturation capacity and b_1, c_1 are constant.

IAST predicts the mixture adsorption equilibriums using single-component adsorption isotherms is defined by[3]

$$S_{CO_2/N_2} = \frac{q_1 / q_2}{p_1 / p_2} \quad (2)$$

where q_1 and q_2 are the CO_2 and N_2 uptake capacities (mmol g^{-1}), respectively; p_1 and p_2 are the specified partial pressure of CO_2 and N_2, respectively.

Table S2. Parameters of single-site Langmuir-Freundlich model by fitting absolute adsorption of pure CO_2 and N_2 at 298 K.

Adsorbent	Adsorbate	A_1 (mmol g^{-1})	b_1 (kPa^{-1})	c_1	R^2
BM-700	CO_2	7.4296	0.01936	0.7181	0.9998
	N_2	2.7431	0.0007673	1.1763	0.9996

Adsorbent	Adsorbate	A_1 (mmol g^{-1})	b_1 (kPa^{-1})	c_1	R^2
BM-800	CO_2	9.5143	0.02428	0.6256	0.9999
	N_2	2.5661	0.002150	1.0080	0.9999

Adsorbent	Adsorbate	A_1 (mmol g^{-1})	b_1 (kPa^{-1})	c_1	R^2
BM-900	CO_2	14.6367	0.01149	0.7247	0.9999
	N_2	1.3649	0.001760	1.2501	0.9994

Adsorbent	Adsorbate	A_1 (mmol g^{-1})	b_1 (kPa^{-1})	c_1	R^2
BM-1000	CO_2	13.2201	0.006430	0.8500	0.9997
	N_2	2.8212	0.001720	1.0474	0.9999

Adsorbent	Adsorbate	A_1 (mmol g^{-1})	b_1 (kPa^{-1})	c_1	R^2
KBM-700	CO_2	8.2085	0.02731	0.6934	0.9997
	N_2	0.8578	0.00174	1.2712	0.9997

Adsorbent	Adsorbate	A_1 (mmol g^{-1})	b_1 (kPa^{-1})	c_1	R^2
KBM-800	CO_2	8.2224	0.02056	0.7554	0.9997
	N_2	1.5429	0.001720	1.1058	0.9999

Adsorbent	Adsorbate	A_1 (mmol g^{-1})	b_1 (kPa^{-1})	c_1	R^2
BM-900	CO_2	8.6469	0.01542	0.7890	0.9996
	N_2	1.8618	0.001770	1.0589	0.9999

Adsorbent	Adsorbate	A_1 (mmol g^{-1})	b_1 (kPa^{-1})	c_1	R^2
KBM-1000	CO_2	7.4612	0.01352	0.8522	0.9995
	N_2	0.7066	0.0006943	1.5642	0.9984

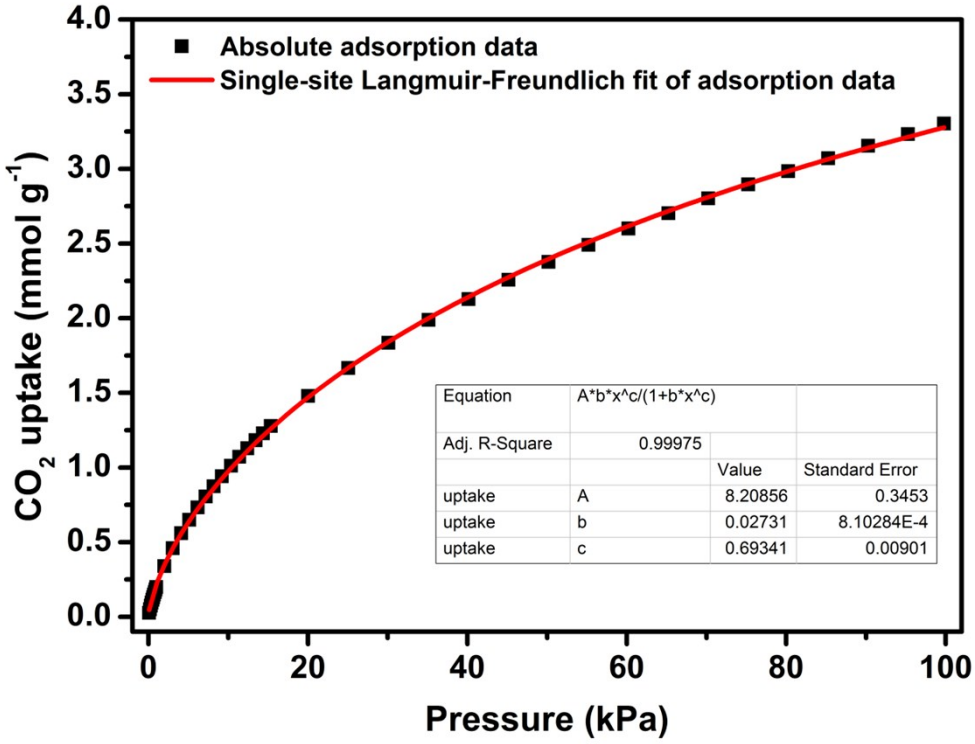

Figure S11. Single-site Langmuir-Freundlich fit of the CO_2 adsorption data on KBM-700 at 298 K, respective fit parameters were used for calculation of the IAST data.

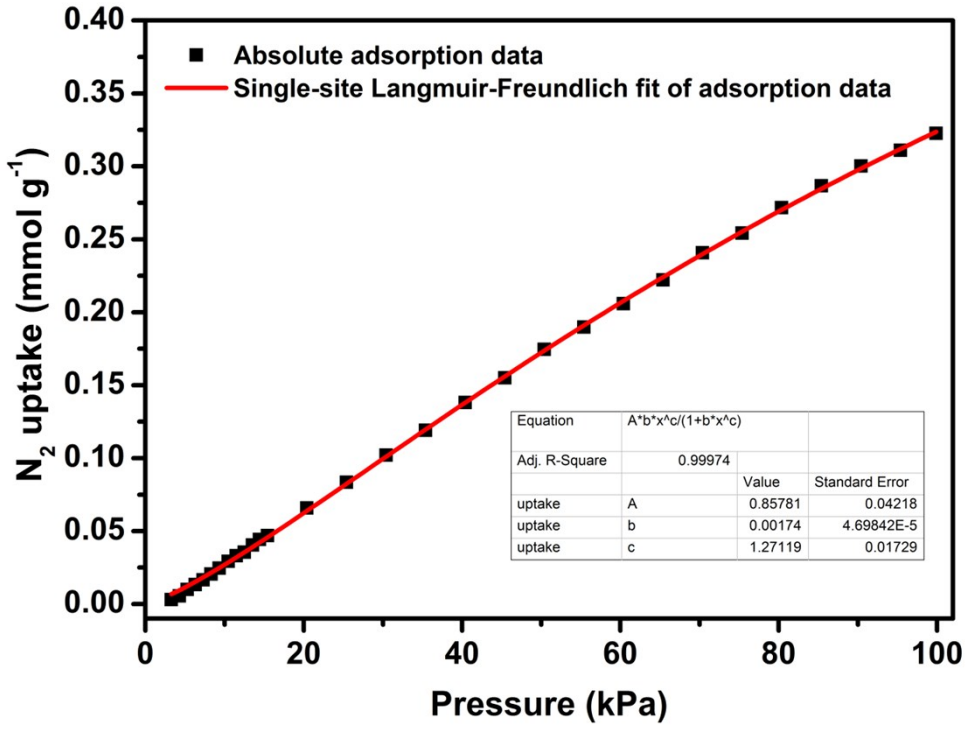

Figure S12. Single-site Langmuir-Freundlich fit of the N_2 adsorption data on KBM-700 at 298 K, respective fit parameters were used for calculation of the IAST data.

Table S3. Summary of textual properties and CO_2 capture performances of **BM-700** and **KBM-700** in comparison to literature reported porous carbon materials.

Sample	S_{BET}[a] $m^2\ g^{-1}$	V_{total}[b] $cm^3\ g^{-1}$	V_{micro}[c] $cm^3\ g^{-1}$	CO_2 uptake (mmol g^{-1})		IAST CO_2/N_2[d]	Reference
				273 K	298 K		
BM-700	682	0.50	0.19	3.52	2.56	23.3	This work
KBM-700	1129	0.55	0.40	4.75	3.29	99.1	This work
nZDC-700	950	-	0.35	5.12	3.51	79	4
IRMOF-3/800	1184	2.01	0.12	3.99	-	38.8	5
MOFC-700	644.9	0.715	-	-	2.12	41	6
mJUC160-900	940	0.44	0.34	5.50	3.50	29	7
SU-MAC-500	941	0.47	0.34	6.03	4.50	39	8
MR-1.5-500	1159	0.49	0.38	5.88	3.56	52.9	9
NC-650-1	1483	0.66	0.57	6.15	4.26	29	10
SNS2-20	2100	1.01	0.93	6.84	4.48	68.9	11
AC-2–635	1381	0.57	0.56	-	3.86	21	12
IBN9-NC1-A	1181	0.73	0.42	-	4.5	32	13

[a] S_{BET} was calculated in the partial pressure (P/P_0) range of 0.05 to 0.2 which gave the best linearity. [b] Total pore volume at relative pressure P/P_0 =0.99. [c] Cumulative micropore volume with diameter $\leqslant$ 2 nm. [d] IAST selectivity at 298 K for the mixture of 0.15/0.85 CO_2 /N_2 at 1 bar.

7. Electrochemical analysis

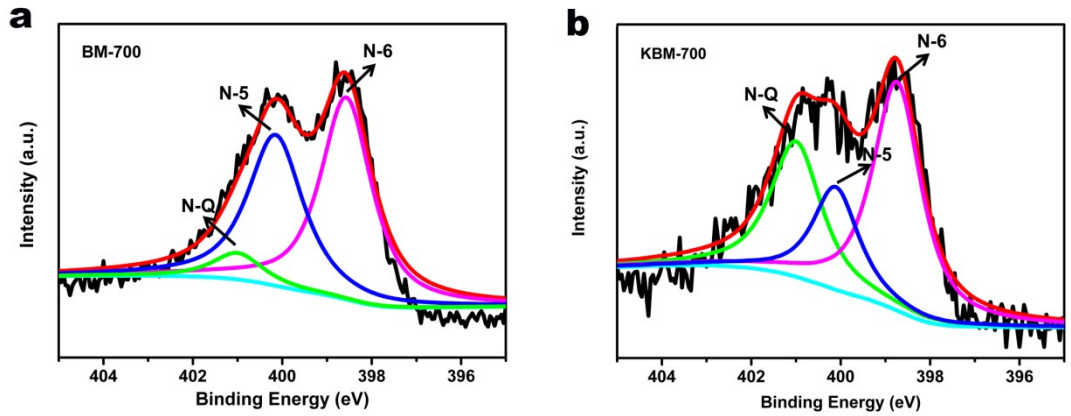

Figure S13. High-resolution XPS spectrum of N 1s XPS peaks of (a) BM-700, (b) KBM-700 samples.

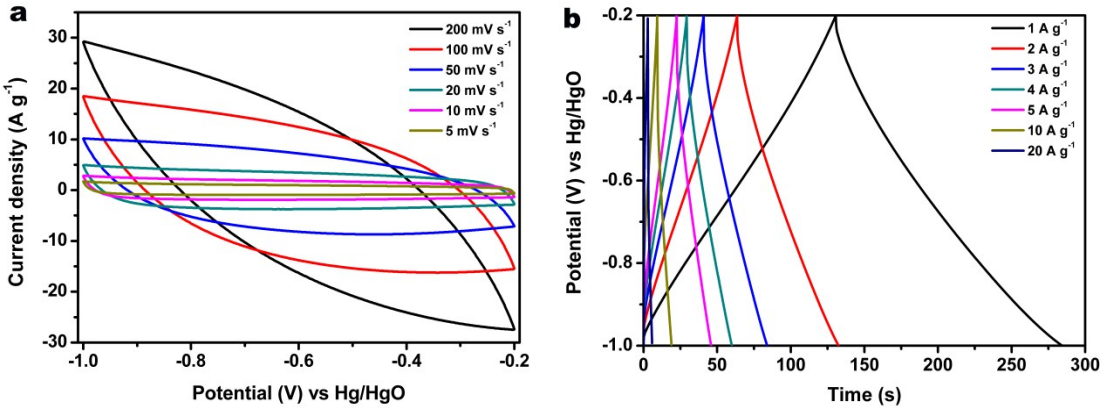

Figure S14. (a) Cyclic voltammograms of BM-700 at different scan rates in 6M KOH; (b) galvanostatic charge–discharge curves of BM-700 at different current densities.

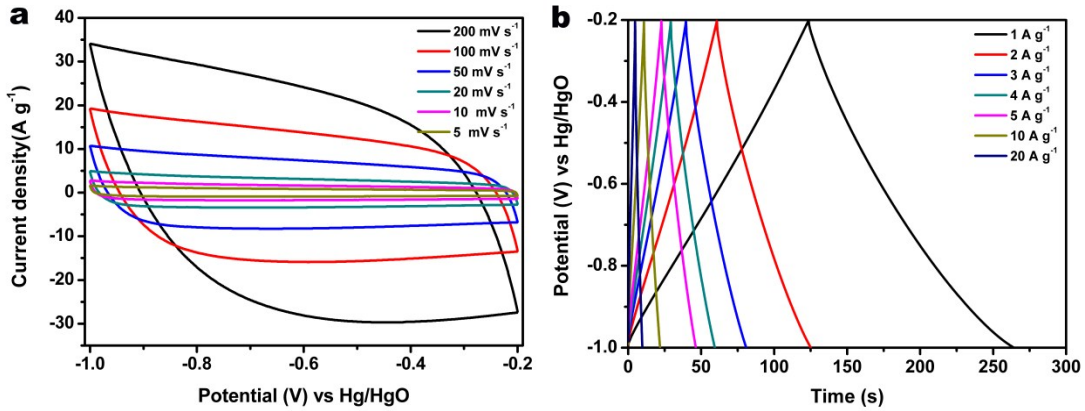

Figure S15. (a) Cyclic voltammograms of BM-800 at different scan rates in 6M KOH; (b) galvanostatic charge–discharge curves of BM-800 at different current densities.

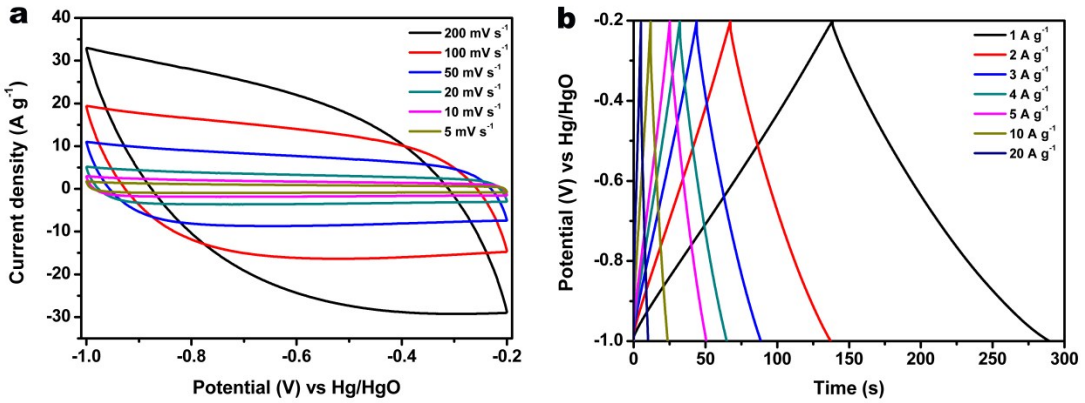

Figure S16. (a) Cyclic voltammograms of BM-900 at different scan rates in 6M KOH; (b) galvanostatic charge–discharge curves of BM-900 at different current densities.

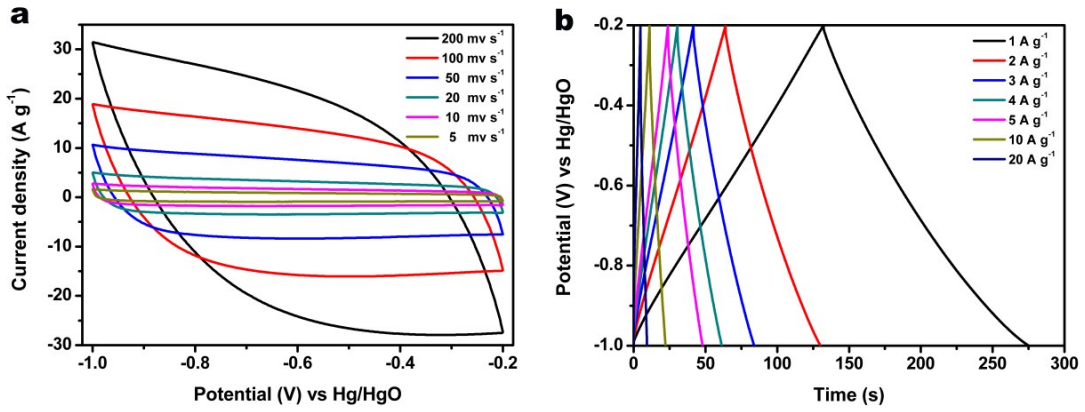

Figure S17. (a) Cyclic voltammograms of BM-1000 at different scan rates in 6M KOH; (b) galvanostatic charge–discharge curves of BM-1000 at different current densities.

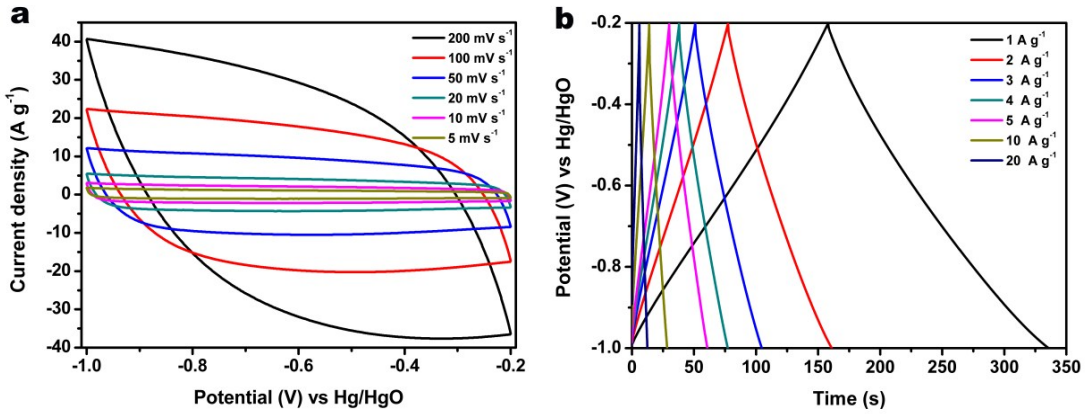

Figure S18. (a) Cyclic voltammograms of KBM-700 at different scan rates in 6M KOH; (b) galvanostatic charge–discharge curves of KBM-700 at different current densities.

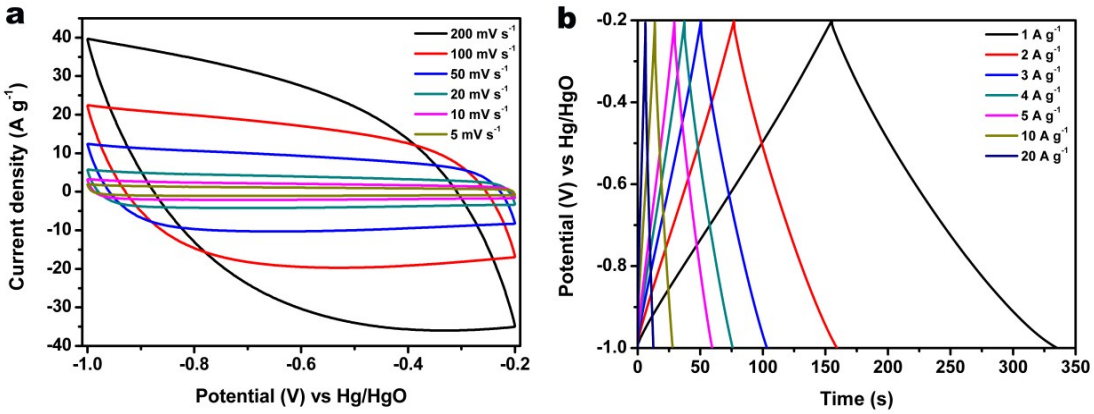

Figure S19. (a) Cyclic voltammograms of KBM-800 at different scan rates in 6M KOH; (b) galvanostatic charge–discharge curves of KBM-800 at different current densities.

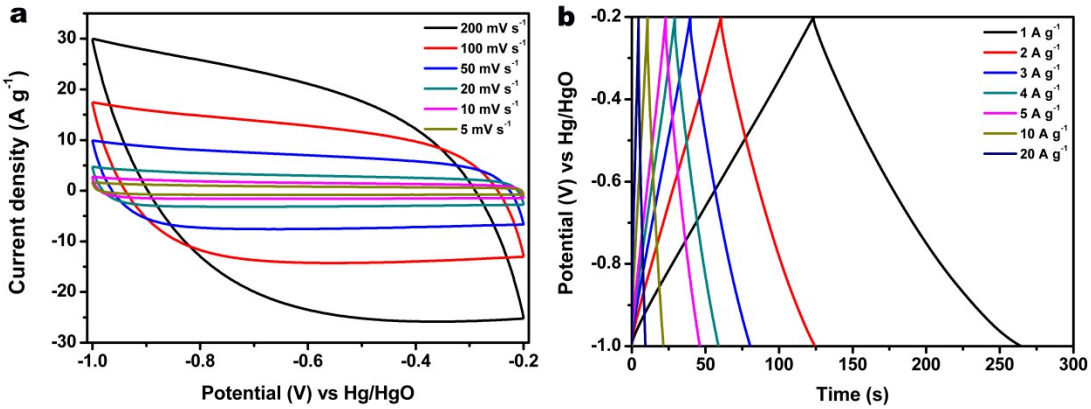

Figure S20. (a) Cyclic voltammograms of KBM-900 at different scan rates in 6M KOH; (b) galvanostatic charge–discharge curves of KBM-900 at different current densities.

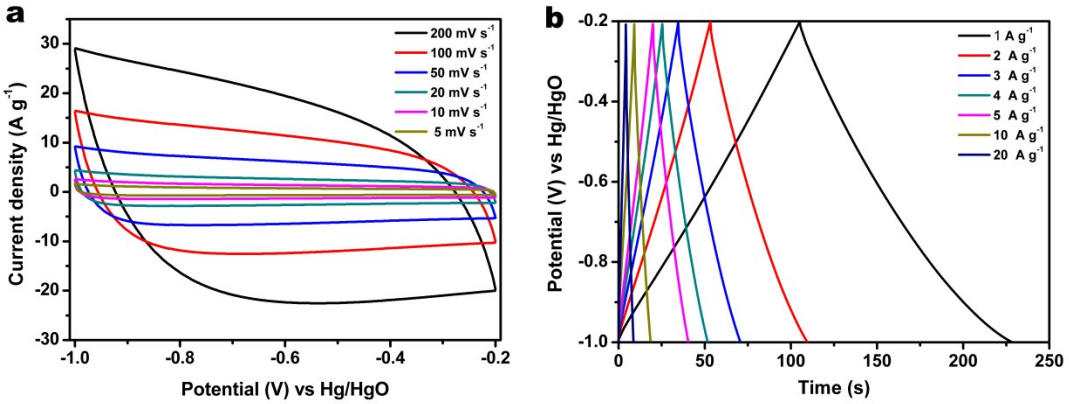

Figure S21. (a) Cyclic voltammograms of KBM-1000 at different scan rates in 6M KOH; (b) galvanostatic charge–discharge curves of KBM-1000 at different current densities.

Table S4. Summary of the supercapacitors performances of **BM-700** and **KBM-700** in comparison to literature reported porous carbon materials

Sample	Current density ($mA\ g^{-1}$)	Specific capacitance ($F\ g^{-1}$)	Electrolyte	Reference
BM-700	1000	192	6 M KOH	This work
KBM-700	1000	230	6 M KOH	This work
Carbon-L-950	100	228	6 M KOH	14
Carbon-ZS	100	285.8	6 M KOH	15
HPCs-0.4	1000	149	6 M KOH	16
NMC-1.5-2	500	229.7	6 M KOH	17
MAC-A	250	274	6 M KOH	18
KF1-90	1000	200	6 M KOH	19
NPC 650	50	222	1 M H_2SO_4	20
C-800	250	200	1 M H_2SO_4	21

References

1. A. L. Myers and J. M. Prausnitz, *AIChE J.*, 1965, **11**, 121-130.
2. A. L. Myers, *Adsorption*, 2003, **9**, 9-16.
3. W. G. Lu, J. P. Sculley, D. Q. Yuan, R. Krishna, Z. W. Wei and H. C. Zhou, *Ang ew. Chem., Int. Ed.*, 2012, **51**, 7480-7484.
4. S. Gadipelli and Z. X. Guo, *ChemSusChem*, 2015, **8**, 2123-2132.
5. S. Ding, Q. Dong, J. Hu, W. Xiao, X. Liu, L. Liao and N. Zhang, *Chem. Commun.*, 2016, **52**, 9757-9760.
6. L. Li, Y. Wang, X. Gu, Q. Yang, and X. Zhao, *Chem. Asian J.*, 2016, **11**, 1913-1920.
7. Y. Pan, M. Xue, M. Chen, Q. Fang, L. Zhu, V. Valtchev and S. Qiu, *Inorg. Chem. Front.*, 2016, **3**, 1112-1118.
8. J. W. F. To, J. He, J. Mei, R. Haghpanah, Z. Chen, T. Kurosawa, S. Chen, W.-G. Bae, L. Pan, J. B.-H. Tok, J. Wilcox and Z. Bao, *J. Am. Chem. Soc.*, 2016, **138**, 1001-1009.
9. H. Cong, M. Zhang, Y. Chen, K. Chen, Y. Hao, Y. Zhao and L. Feng, *Carbon*, 2015, **92**, 297-304.
10. M. Yang, L. Guo, G. Hu, X. Hu, L. Xu, J. Chen, W. Dai and M. Fan, *Environ. Sci. Technol.*, 2015, **49**, 7063-7070.
11. Y. K. Kim, G. M. Kim and J. W. Lee, *J. Mater. Chem. A*, 2015, **3**, 10919-10927.
12. X. Fan, L. Zhang, G. Zhang, Z. Shu and J. Shi, *Carbon*, 2013, **61**, 423-430.
13. Y. Zhao, L. Zhao, K. X. Yao, Y. Yang, Q. Zhang and Y. Han, *J. Mater. Chem.*, 2012, **22**, 19726-19731
14. P. Zhang, F. Sun, Z. Shen and D. Cao, *J. Mater. Chem. A*, 2014, **2**, 12873-12880.

15. S. Zhong, C. Zhan and D. Cao, *Carbon*, 2015, **85**, 51-59.
16. S. Mo, Z. Sun, X. Huang, W. Zou, J. Chen and D. Yuan, *Synth. Met.*, 2012, **162**, 85-88.
17. Q. Shi, R. Zhang, Y. Lv, Y. Deng, A. A. Elzatahrya and D. Zhao, *Carbon*, 2015, **84**, 335-346.
18. J. Hu, H. Wang, Q. Gao and H. Guo, *Carbon*, 2010, **48**, 3599-3606.
19. Y. Lv, F. Zhang, Y. Dou, Y. Zhai, J. Wang, H. Liu, Y. Xia, B. Tu and D. Zhao, *J. Mater. Chem.*, 2012, **22**, 93-99.
20. B. Liu, H. Shioyama, H. Jiang, X. Zhang and Q. Xu, *Carbon*, 2010, **48**, 456-463.
21. H.-L. Jiang, B. Liu, Y.-Q. Lan, K. Kuratani, T. Akita, H. Shioyama, F. Zong and Q. Xu, *J. Am. Chem. Soc.*, 2011,**133**, 11854-11857.